Spin coherence lifetime extension in Tm^{3+}:YAG through dynamical decoupling

M. F. Pascual-Winter, R.-C. Tongning, T. Chanelière, and J.-L. Le Gouët
Laboratoire Aimé Cotton, CNRS-UPR 3321, Université Paris-Sud, Bâtiment 505, Campus Universitaire, 91405 Orsay Cedex, France
(Received 8 August 2012; published 6 November 2012)

We report on spin coherence lifetime extension in Tm^{3+}:YAG obtained through dynamically decoupling the thulium spins from their magnetic environment. The coherence lifetime reached with a Carr-Purcell-Meiboom-Gill sequence revealed a 450-fold extension [$\sim(230 \pm 30)$ ms] with respect to previously measured values. Comparison to a simple theoretical model allowed us to estimate the correlation time of the fluctuations of the ground-level transition frequency to (172 ± 30) μs at 1.7 K. For attaining efficient decoupling sequences, we developed a strategy inspired by the *zero-first-order Zeeman* effect to minimize the large inhomogeneous broadening of the ground-level spin transition.

DOI: 10.1103/PhysRevB.86.184301 PACS number(s): 03.67.Pp, 76.30.Kg, 42.50.Gy, 82.56.Jn

I. INTRODUCTION

The building block of quantum information is the superposition state between two states of a quantum system, known as a qubit. The success of a certain qubit technology depends strongly on how long the quantum character of the state holds. Reaching long coherence lifetimes of the quantum system is thus a main issue. This is even a more crucial concern when it comes to quantum memories, whose goal is to keep the information as long as possible, respecting faithfully the quantum character of the stored qubit.[1,2] Rare-earth-based systems are excellent prospects of quantum memories thanks to their long coherence lifetime, T_2, at low temperature, both of optical and hyperfine transitions. In particular, rare-earth-ion-doped crystals (REIDC) present the additional advantage of providing motionless centers without any trade-off loss of T_2.[3] Therefore, rare-earth long T_2's can be fully exploited in REIDC since the storage time of the device is not limited by atomic motion, as it is in atomic vapors. Even though storage protocols make use of the longer-lived ground-state hyperfine (spin) superposition states, the extension of T_2 from the $\sim$100 μs to the $\sim$100 ms scale, or even the second, is desirable in REIDC.

At low temperature, spin decoherence of some materials such as Tm^{3+}:YAG is ruled by the interaction of the rare-earth spins with the fluctuating magnetic field produced by the nuclear spins of the host matrix. Different techniques have been developed to decouple the system from its environment in seeking to extend T_2. The one known as *spin locking* consists of applying a strong radio-frequency (rf) magnetic field parallel to the spins and tuned to the spin transition.[4,5] However, good tuning to the spin transition is not available in inhomogeneously broadened systems, such as REIDC. Besides, when the spin coherences result from the transformation of optical ones—as in quantum storage protocols—the initial parallelism between the spins and rf field cannot be ensured for all of the spins in the ensemble. Therefore, the spin-locking extension of T_2 is not compatible with quantum storage.

A successful technique recently implemented[6,7] on REIDCs makes use of the *zero-first-order Zeeman* (ZEFOZ) effect. It consists of carefully looking for a static magnetic field that is precisely sized and oriented such that the gradient of the ground-level splitting with respect to the magnetic field coordinates vanishes. As a result, the spins are insensitive (in first order) to the environment-induced magnetic field fluctuations. This has led to T_2 extensions of up to three orders of magnitude.[7] Nevertheless, ZEFOZ critical points are available only in REIDCs that present a zero-field hyperfine splitting.[6]

Dynamical decoupling (DD) is a broadly used technique for the extension of T_2 (for a review, see Ref. 8). Based on the Hahn spin echo,[9] it was first applied in the context of NMR for high-precision spectroscopy.[10] More recently, the interest in preserving the coherence in quantum information qubits has been pointed out.[11–14] The simplest, and still highly efficient, DD scheme is the Carr-Purcell-Meiboom-Gill (CPMG) sequence.[15,16] For an initial coherence state known at $t = 0$, it consists of the application of π pulses separated by intervals of duration τ, with the first pulse arriving at $t = \tau/2$ [see Fig. 5(a)]. The phase of the π pulses alternates between 0 and π in order to compensate for pulse imperfections. Disregarding the alternating phase, the scheme can be alternatively seen as the repetition of an elementary sequence [dashed rectangle in Fig. 5(a)] composed by a $\tau/2$-long free evolution interval, a π pulse, and another $\tau/2$-long free evolution interval. If the spin level splitting does not change significantly during the duration τ of the total free evolution time in the elementary sequence, then the spin coherence will be found at known states at the end of each elementary sequence, i.e., at $t = j\tau$, with j as the elementary sequence index. These states are either the initial state, for j even, or a π-phase-shifted state, for j odd. Hence, the coherence can be preserved as long as the π pulses are applied. The challenge consists in increasing the π-pulse rate in order to compensate for the effect of the environment before this one suffers from significant reconfiguration.

Experimental realizations of DD have yielded remarkable results, especially in molecules,[17] trapped ions,[18] and nitrogen-vacancy centers in diamond.[19] Fraval and coworkers have successfully applied the CPMG sequence to Pr^{3+}:Y_2SiO_5,[6] which is the most thoroughly studied REIDC for quantum memory applications. A combination of the ZEFOZ and CPMG techniques yielded a coherence lifetime over 30 s long.

Thulium-doped YAG (Tm^{3+}:YAG) has been identified as an attractive REIDC thanks mainly to its diode-laser-accessible optical line (793 nm) and its very simple level structure under static magnetic field (two ground and two excited sublevels).[20] Its large optical inhomogeneous broadening (20 GHz) can also

be useful for broadband applications such as light storage.[21] In recent years, it has been actively investigated in the prospect of quantum storage.[21–29] However, the degeneracy of its hyperfine sublevels due to quenching of the total angular momentum[30] does not allow use of the ZEFOZ technique. T_2 extension in Tm^{3+}:YAG must thus rely on DD only. Nevertheless, the simple CPMG sequence cannot be straightforwardly transposed to Tm^{3+}:YAG. The reason, as we will discuss in detail below, is its large spin-transition inhomogeneous broadening (∼20 times broader than in Pr^{3+}:Y_2SiO_5), which imposes high power constraints to the rf field. Hence, a strategy for minimizing the spin inhomogeneous linewidth is compulsory.

This paper reports on T_2 extension through CPMG-based DD in Tm^{3+}:YAG. In Sec. II, we will discuss the problem related to inhomogeneous broadening and we will describe a ZEFOZ-inspired strategy for minimizing the broadening. Three experimental sections follow. In Sec. III A, we will characterize the system (i.e., resulting inhomogeneous broadening, nonextended T_2, etc). In Sec. III B, we will present results on the viability of the CPMG sequence in Tm^{3+}:YAG. Finally, Sec. III C will be dedicated to T_2 extension through DD. The Appendix describes a theoretical model that fits our experimental data.

II. MINIMIZATION OF THE INHOMOGENEOUS BROADENING

A CPMG sequence is based on the application of successive rf π pulses to a spin ensemble. In order to act over the whole ensemble, the hard pulse spectrum must cover that of the spins. Thus, rather short pulses are necessary. At the same time, the condition of pulse area equal to π must be fulfilled. Therefore, the broader the atomic spectrum, the higher the requirements on pulse intensity.

As we said, the CPMG sequence has been successfully applied to Pr^{3+}:Y_2SiO_5. In that crystal, the inhomogeneous hyperfine linewidth, Γ_{inh}, is as narrow as 15–30 kHz.[31,32] A square π pulse of Rabi angular frequency Ω has a bandwidth of the order of Ω. In the case of Γ_{inh} of the order of some tens of kHz, reasonable rf powers can produce rf pulses able to act on a bandwidth several times broader than Γ_{inh}. Pulses need not be shorter than a few tens of microseconds. In other words, efficient π pulses are readily affordable for Pr^{3+}:Y_2SiO_5.

The scenario is quite different for Tm^{3+}:YAG. As reported in previous experiments,[29] $\Gamma_{inh} \simeq 500$ kHz, which makes rf π pulses much more challenging. Indeed, for the experimental conditions of Ref. 29, the 280 kHz Rabi frequency obtained with a 65 W rf power yields a π pulse bandwidth far too narrow to expect an efficient CPMG sequence. Hence, a strategy for minimizing Γ_{inh} is to be developed for Tm^{3+}:YAG.

Let us first address the reason behind this large Γ_{inh}. The splitting of hyperfine sublevels is achievable in Tm^{3+}:YAG through the application of an external magnetic field $\mathbf{B}$. For a given $\mathbf{B}$, the energy difference between sublevels is determined by the gyromagnetic tensor γ. It is actually the strong anisotropy of this tensor in Tm^{3+}:YAG ($\gamma_y \gg \gamma_x, \gamma_z$; x, y, z to be defined later) that is responsible for high Γ_{inh}. Let us describe in a few words how this happens (we will go through the details later): the high anisotropy of the gyromagnetic tensor entails a strong sensitivity of the sublevel splitting angular frequency Δ to the orientation of $\mathbf{B}$. Either spatial inhomogeneities in the field or variations in the lattice orientation within the sample make the magnetic field orientation seen by the Tm^{3+} ions vary slightly from one ion site to another. Because of the high anisotropy of the gyromagnetic tensor, these slight variations entail strong ones in Δ. This results in a span of values for Δ that adds up to give a line broadening. The strategy we propose to minimize this broadening is to look for a particular orientation of $\mathbf{B}$ where the sensitivity of Δ to the orientation is minimum.

Although driven by a different motivation, this approach is quite similar to the ZEFOZ technique. In that case, the procedure consists of searching for a specific $\mathbf{B}$ whose orientation *and magnitude* satisfy $\nabla_B \Delta = 0$,[6,7,33] where ∇_B is the gradient with respect to the magnetic field coordinates. In the problem we are interested in, of course, an increase of T_2 through the ZEFOZ effect would be welcome, but our main concern is still to minimize Γ_{inh} in order to maximize the efficiency of π pulses. The procedure here also searches for a minimization of the sensitivity of Δ to $\mathbf{B}$. However, full vanishing of $\nabla_B \Delta$ is possible only in systems that present a zero-field hyperfine splitting.[6] This is not the case of Tm^{3+}:YAG, where hyperfine sublevels are degenerate because of quenching of the total angular momentum.[30] Thus, a full ZEFOZ effect is not possible in Tm^{3+}:YAG. Nevertheless, *partial* ZEFOZ, that is, vanishing derivatives of Δ with respect to *two* of the magnetic field coordinates, is still possible, as we will see in detail below.

In the presence of a magnetic field, the Hamiltonian for Tm^{3+} ions takes a simple form for sites of D_2 point symmetry, which is the case of Tm^{3+} substituting for Y^{3+} in a YAG matrix. It can be expressed as a nuclear Zeeman term,[34]

$$\mathcal{H}' = -\hbar\gamma_n \mathbf{B}_{\text{eff}} \cdot \mathbf{I}, \tag{1}$$

with an effective magnetic field given by

$$\mathbf{B}_{\text{eff}} = (\gamma_x B_x \hat{\mathbf{x}} + \gamma_y B_y \hat{\mathbf{y}} + \gamma_z B_z \hat{\mathbf{z}})/\gamma_n. \tag{2}$$

The quantities $\mathbf{I}$ and γ_n are the nuclear spin operator and gyromagnetic ratio, respectively, and $\hat{\mathbf{x}}$, $\hat{\mathbf{y}}$, $\hat{\mathbf{z}}$ are the three orthogonal twofold axes of the D_2 point group. γ_x, γ_y, γ_z are defined as the eigenvalues of the rank-2 tensor,

$$\gamma_{\alpha\beta} = \gamma_n \mathbb{1} + \frac{2 g_J \mu_B A_J}{\hbar} \sum_{n=1}^{2J+1} \frac{\langle 0|J_\alpha|n\rangle\langle n|J_\beta|0\rangle}{E_n - E_0}, \tag{3}$$

where μ_B is Bohr's magneton, g_J is the Landé factor for the manifold of total angular momentum J, A_J is the hyperfine interaction parameter,[34] and E_n is the energy of the eigenstate $|n\rangle$ of the Hamiltonian comprising the free ion and crystal-field terms. In the case of D_2 point-group symmetry, $\gamma_{\alpha\beta}$ is diagonal in the basis $\{\hat{\mathbf{x}}, \hat{\mathbf{y}}, \hat{\mathbf{z}}\}$.[35] The splitting between the eigenstates of the Hamiltonian (1) is given by

$$\Delta(B_x, B_y, B_z) = \left(\gamma_x^2 B_x^2 + \gamma_y^2 B_y^2 + \gamma_z^2 B_z^2\right)^{1/2}, \tag{4}$$

$$\Delta(B, \theta, \phi) = \Delta_B(\theta, \phi) B, \tag{5}$$

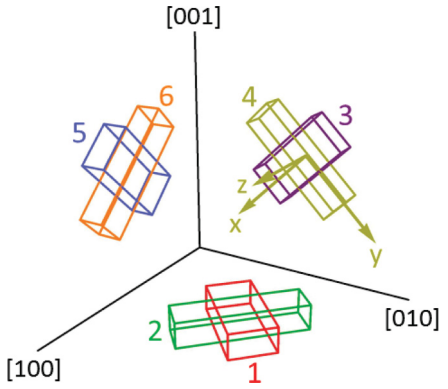

FIG. 1. (Color online) Orientations of the six orientationally distinct sites of the Y^{3+} ion in the YAG crystal lattice.[36] Each parallelepiped represents the local D_2 symmetry for one of the sites. The $\hat{\mathbf{x}}$, $\hat{\mathbf{y}}$, $\hat{\mathbf{z}}$ axis are the local axis for site 4.

where $B = (B_x^2 + B_y^2 + B_z^2)^{1/2}$ and θ and ϕ are spherical coordinates for the polar and azimuthal angles, respectively, with respect to some convenient Cartesian reference frame.

Y^{3+} ions in the YAG lattice occupy six sites that are equivalent in terms of their local environment but distinct in terms of the orientation of this environment, i.e., the axes of the D_2 point group are differently oriented (see Ref. 36 and references therein). The site orientations are sketched in Fig. 1 by six parallelepipeds that represent the possible orientations of the D_2 symmetry. When an external field is applied, its effect on each site must be treated separately. To study the behavior of $\Delta_B(\theta,\phi)$, we will consider the site for which $\hat{\mathbf{x}}$, $\hat{\mathbf{y}}$, $\hat{\mathbf{z}}$ are oriented along $[0\bar{1}\bar{1}]$, $[01\bar{1}]$, [100], respectively; this is the site "4" as labeled in Fig. 1. Justification for this choice will be given later. In Fig. 2(a), the strong variations of Δ_B as a function of (θ,ϕ) reflect the high anisotropy of γ_x, γ_y, and γ_z. For the figure, we used the values $\gamma_y = (403 \pm 3)$ MHz/T, $\gamma_x = 0.045\gamma_y$, and $\gamma_z = 0.017\gamma_y$ that are compatible with the experimental observations of Ref. 22. The angles θ and ϕ have been taken with respect to the axis {[100],[010],[001]} of the YAG Bravais lattice.

Our aim is to minimize Γ_{inh}. For that, our strategy is to look for a magnetic field orientation (θ,ϕ) for which the splitting sensitivity to the magnetic field is minimum. We see in Fig. 2(a) that $\Delta_B(\theta,\phi)$ displays both maxima and minima that meet this criterion. The question now is what exact field orientation to choose. For example, is it better to choose a maximum or a minimum? A minimum seems to be a better choice since inhomogeneous broadening resulting from fluctuations in the *magnitude* of the magnetic field would be as small as possible. In other words, the situation would be closer to a full cancellation of $\nabla_B \Delta$. However, that is not the only criterion to take into account.

As we said before, the aim of keeping Γ_{inh} small is to lower the constraint on π-pulse bandwidth, and thus on π-pulse duration, so that the pulses produced with the available rf power will act efficiently over the whole Γ_{inh}. Of course, rf power is not the good parameter to look at; it is rather its associated Rabi frequency Ω which comes into play. Usually, it is the rf field component orthogonal to the static field that determines Ω. For Hamiltonian terms such as (1), both for $\mathbf{B}$

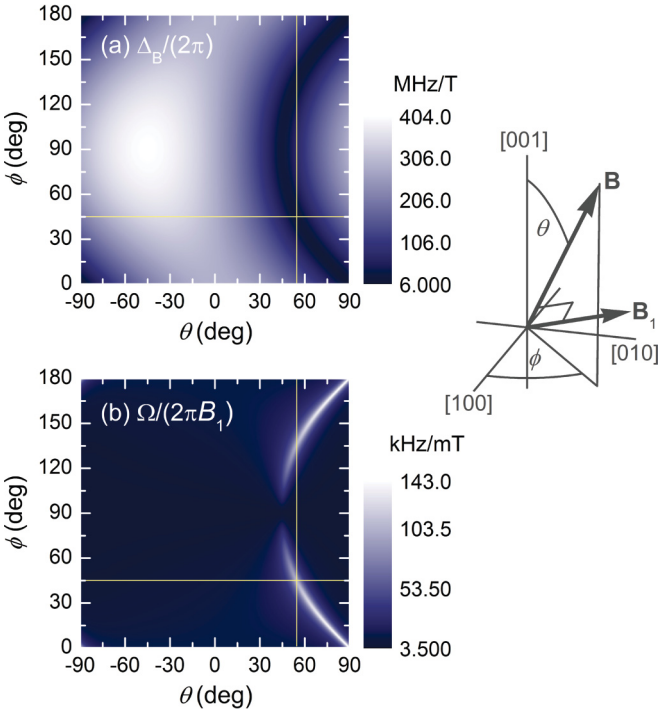

FIG. 2. (Color online) (a) Spin sublevel splitting per tesla (T) and (b) Rabi frequency per millitesla (mT) as a function of the orientation of the static magnetic field $\mathbf{B}$ with respect to the {[100],[010],[001]} reference frame of the YAG crystal. The rf field $\mathbf{B}_1$ is always orthogonal to $\mathbf{B}$, and contained in the (001) plane. The lines indicate the orientation chosen for the experiments: $(\theta = 54.8°, \phi = 45°)$, which ensures low Γ_{inh} and high Ω.

and for the rf field $\mathbf{B}_1$, what counts is the component of $\mathbf{B}_{1,\text{eff}}$ orthogonal to $\mathbf{B}_{\text{eff}}$ [$\mathbf{B}_{1,\text{eff}}$ is defined as in Eq. (2) by substituting B_x, B_y, B_z with $B_{1,x}$, $B_{1,y}$, $B_{1,z}$]. In our experimental setup, the fields $\mathbf{B}$ and $\mathbf{B}_1$ are generated by two coils perpendicular to one another. As the coils are fixed, the static field orientation is actually performed by rotating the crystal rather than the magnetic field. Therefore, the orientations of $\mathbf{B}$ and $\mathbf{B}_1$ cannot be varied independently. When choosing the orientation of $\mathbf{B}$ (or rather that of the crystal), care must be taken since, as a result of the strong gyromagnetic tensor anisotropy, Ω may vary significantly.

In Fig. 2(b), we present the behavior of Ω as a function of the angles θ and ϕ that determine the orientation of $\mathbf{B}$ and, consequently, that of $\mathbf{B}_1$. The experimental setup fixes the rf field orientation as $\mathbf{B}_1/B_1 = (-\sin\phi, \cos\phi, 0)$ with respect to the crystal frame {[100],[010],[001]}. It is clear from the figure that a non-negligible Ω is observed only at very specific orientations. The region of high Ω coincides with the "C" -shaped minimum line observed for $\Delta_B(\theta,\phi)$ in Fig. 2(a). This is, of course, not a coincidence; it results from the particular anisotropy of γ_{ab}. To understand this statement, we need to bear in mind that as soon as a given field has a non-negligible y component, its associated *effective* field is (almost) parallel to $\hat{\mathbf{y}}$ because of $\gamma_y \gg \gamma_x, \gamma_z$ [see Eq. (2)]. Thus, even though $\mathbf{B} \perp \mathbf{B}_1$, it happens that $\mathbf{B}_{\text{eff}} \parallel \mathbf{B}_{1,\text{eff}}$ for most field orientations. Ω is determined by the component of $\mathbf{B}_{1,\text{eff}}$ orthogonal to $\mathbf{B}_{\text{eff}}$. The orthogonality only happens if either (i) $B_y \simeq 0$ or (ii) $B_{1,y} \simeq 0$. In case (ii), however, $|\mathbf{B}_{1,\text{eff}}|$ is strongly diminished

as a result of $\gamma_x,\gamma_z \ll \gamma_y$. Therefore, only case (i) displays high Ω. At the same time, as $\gamma_y \gg \gamma_x,\gamma_z$, fulfilling (i) results in minimizing Δ [see Eq. (4)]. That is why the regions of minimum Δ and high Ω coincide in Fig. 2.

The arguments just given answer the question of whether to choose a maximum or a minimum of $\Delta_B(\theta,\phi)$ when aiming at minimizing Γ_{inh}. To further specify the orientation (θ,ϕ) of **B**, it can be shown that at $\phi = 45°$, site 6 presents the same Δ and Ω as site 4 described above. This permits one to double the experimental signal by addressing two sites at a time, and, at the same time, avoid a double-valued Ω. Once $\phi = 45°$ is set, θ is automatically fixed by selecting the minimum of $\Delta_B(\theta,45°)$. It occurs at $\theta = 54.8°$. For the resulting orientation $(\theta = 54.8°,\phi = 45°)$, indicated in Fig. 2 by crossed lines, we expect $\Delta_B = 15.3$ MHz/T and $\Omega/(2\pi B_1) = 101$ kHz/mT. Static and rf fields of the order of a few T and mT, respectively, are perfectly compatible with the experimental capabilities. From previous experiments performed at $(\theta = 49°,\phi = 45°)$, we estimated the angular uncertainty in our crystal to be $\sim 0.3°$. The corresponding Γ_{inh} obtained theoretically is 28 kHz. The set of values we have found for Γ_{inh}, Δ, and Ω makes CPMG sequences experimentally feasible in Tm^{3+}:YAG.

As regards the remaining sites, they will not participate in the experiment. Sites 1, 3, and 5 display a spin-transition frequency far from resonance for the chosen field orientation. In addition, sites 3 and 5 present a forbidden optical dipole moment for the electric-field polarization (parallel to $[11\bar{1}]$) that we will use for initializing and reading out the system. That is also the case for site 2.

Here we have limited our analysis to site 4, mentioning at the end that site 6 returns equal values of Δ_B and Ω for the specific orientation $(\theta = 54.8°,\phi = 45°)$. Actually, the same situation is found for sites 3 and 5 at the orientation $(\theta = -54.8°,\phi = 45°)$. We could have chosen to work at this orientation, where just the indexes of the sites participating in the experiment would have changed. Our experimental configuration (i.e., geometry of the magnetic coils, light propagation axis, and orientation of the facets of our crystal) does not allow us to work effectively with site 1 (low Ω) and it does not allow any optical addressing to site 2 at all (light polarization orthogonal to the electric dipole). It is worth mentioning that if the orientations of the magnetic fields could be varied independently and at will, and if the crystal facets could be chosen arbitrarily, then any pair of sites of common index parity could be picked to participate in the experiment. Alternatively, one could choose to work with one site only, obtaining higher Ω but lower signal.

III. EXPERIMENTS AND DISCUSSION

A. Characterization

The experiments were carried out in a 0.1% at Tm^{3+}:YAG crystal cooled down to 1.7 K in a liquid Helium cryostat. Superconductive coils generate a static magnetic field which lifts the spin degeneracy, resulting in a four-level system composed of two ground states and two excited states. The static magnetic field is oriented as described in the previous section. As in Ref. 29, the spin transition is resonantly driven by a phase-controlled rf magnetic field. A 10-turn coil, 20 mm long and 10 mm in diameter, conveys the magnetic excitation to the crystal sitting at its center. The rf signal generated by an arbitrary wave generator (Tektronix AWG5004) passes through a pulsed amplifier (TOMCO BT00500-AlphaSA). A $\sim$600-kHz-bandwidth rf resonant circuit further amplifies the rf current fed to the coil. The static magnetic field magnitude, close to 1 T, is chosen to produce a ground-level spitting tuned to the rf circuit resonance (15.1 MHz). The light beam, emerging from an extended cavity diode laser and time shaped by acousto-optic modulators, is resonant with the optical transition of the system at 793 nm. It is used for initializing and probing the system. It propagates along the $[\bar{1}10]$ direction with polarization parallel to $[11\bar{1}]$. The opacity of the $L = 5$-mm-long sample has been measured to be $\alpha L = 0.9$.

First of all, we will experimentally verify the reduction of Γ_{inh} and the availability of a reasonably high Ω. A hole-burning experiment [see Fig. 3(a)] revealed a full width at half maximum of the spin-transition antihole of 105 kHz. This is well below the previously reported value of $\simeq$500 kHz,[29] showing that the strategy for minimizing Γ_{inh} has been fruitful. In the absence of inhomogeneous broadening, the antihole width should coincide with that of the central hole. The latter is measured to be 93 kHz. The $\sim$10 kHz growth from the hole to the antihole is consistent with the expected value of Γ_{inh}. The hole width by far exceeds the homogeneous width of the optical transition, of the order of a few kHz only.[20] Since the hole has been deeply burnt, down to the transparency level, saturation may explain the large observed broadening, which is a typical feature in similar situations. The laser linewidth, reduced to

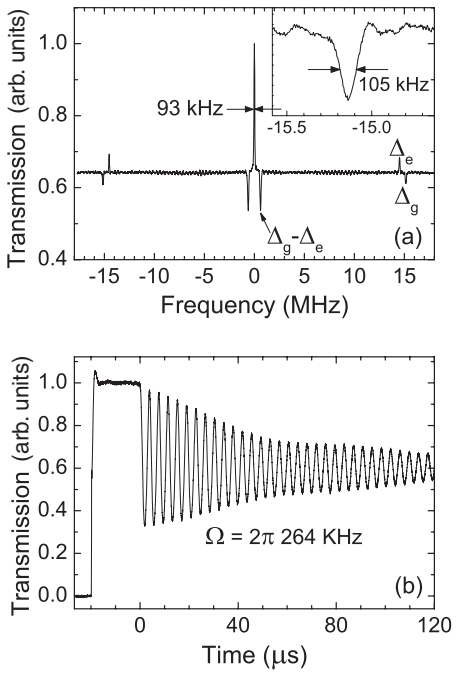

FIG. 3. (a) Hole-burning spectrum. Ground level splitting antiholes (Δ_g), excited level splitting holes (Δ_e), and mixed antiholes ($\Delta_g - \Delta_e$) are observed in addition to the central hole. The Δ_g antihole is 105 kHz wide. (b) Spin nutation experiment. The rf field is turned on at $t = 0$. The spins nutate at a Rabi angular frequency of $2\pi \times 264$ kHz.

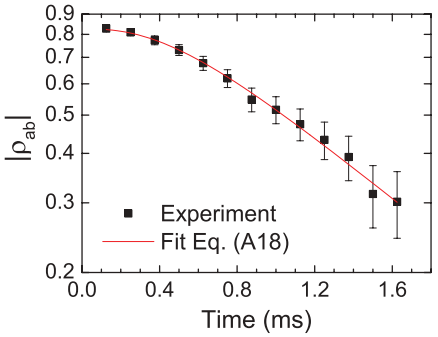

FIG. 4. (Color online) Spin-echo experiment. $|\rho_{ab}|$ is obtained from the quantity $\ln(I_f/I_{ref})/\ln(I_i/I_{ref})$, where I_i and I_f are the transmitted probe intensities before and after the rf sequence, respectively, and I_{ref} is a reference intensity for a known population difference (typically 0). The fit returns the parameters $\sigma_\Delta/(2\pi) = (2.3 \pm 0.2)$ kHz and $\tau_c = (172 \pm 30)$ μs.

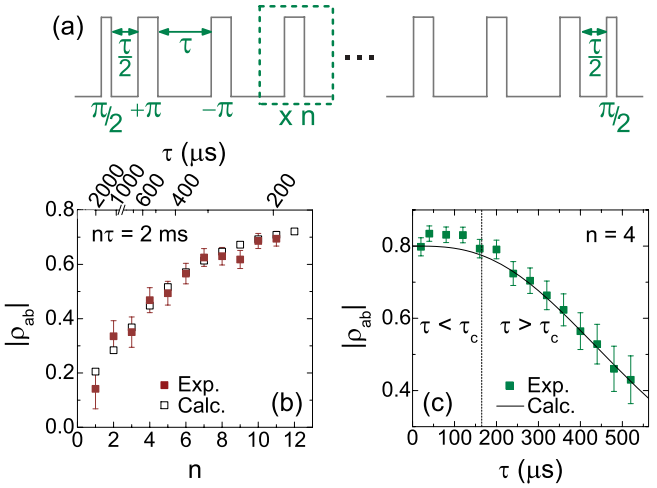

FIG. 5. (Color online) (a) Scheme of the CPMG sequence. The signs "+" and "−" that precede the label of the π pulses refer to the pulse phase, corresponding to 0 or π, respectively. n and τ stand for the number of π pulses and the time interval between them. (b), (c) Coherence recovered after a CPMG sequence with (b) fixed free evolution time $n\tau = 2$ ms and increasing n, or (c) fixed $n = 4$ and increasing τ. The calculated data are obtained from Eq. (A15) with $\sigma_\Delta/(2\pi) = 2.3$ kHz and $\tau_c = 172$ μs.

less than 1 kHz over 10 ms by locking to a Fabry-Pérot interferometer, should not affect the hole width, but the drift of the reference cavity during the burning process might also add to hole and antihole broadening. An imperfect orientation of **B**, differing slightly from ($\theta = 54.8°, \phi = 45°$), might also contribute to Γ_{inh} being larger than expected. In any case, our experimental result fixes an upper bound for Γ_{inh}. As regards Ω, we have performed a spin nutation experiment [see Fig. 3(b)] that yielded $\Omega/(2\pi) = 264$ kHz for a rf power (∼27 W), which is well below the maximum capability of our amplifier. With this value, square-shaped π pulses as short as 1.8 μs are possible. This gives a pulse bandwidth of $\sim\Omega$ that is comfortably larger than Γ_{inh}. These are the parameters to be used in the sequences of the CPMG experiments to be discussed.

In order to weigh the impact of the CPMG sequence on the extension of T_2, we have measured the latter by means of an optically detected spin-echo experiment. For the optical detection, a $\pi/2$ pulse is applied at the end of the spin-echo sequence [see Fig. 5(a) for a sketch; consider $n = 1$]. It is aimed at converting the coherence ρ_{ab} back into an optically detectable population difference. The transmission of a probe beam is measured prior and post application of the rf spin-echo sequence. The relevant experimental information is contained in the comparison between the initial and final probe intensity. The results are presented in Fig. 4. We observe a nonlinear behavior, with the nonlinear character being more pronounced at short times. This tells us that at the time scale of Fig. 4, we have not yet reached the limit $t \gg \tau_c$ in which $|\rho_{ab}|$ decays in an exponential fashion. τ_c is the correlation time of the fluctuations in Δ induced by the environmental aluminium spins. We also note that $|\rho_{ab}|$ does not reach unity for times approaching to zero. This can be due to imperfect matching of the rf frequency to the spin transition. Finite Γ_{inh} also contributes to matching imperfections. We have developed a theoretical model for calculating the evolution of ρ_{ab} during the CPMG sequence. Details can be found in the Appendix. This model reduces to the case of the spin echo when the number of π pulses in the sequence is set to one. The expression for ρ_{ab} is given in Eq. (A18). The parameters of the model are τ_c and the standard deviation of the fluctuation in Δ, σ_Δ (a global offset is also included as a parameter). We have fitted the model to the experimental data. The result is represented by the line in Fig. 4. The agreement with the experiment is satisfactory. The fitting procedure yields $\sigma_\Delta/(2\pi) = (2.3 \pm 0.2)$ kHz and $\tau_c = (172 \pm 30)$ μs. Not only are these values interesting themselves, but they also permit one to estimate T_2 even if the time scale of our experiment is not long enough to appreciate the exponential decay. The estimation is performed through the expression $T_2^{-1} = \sigma_\Delta^2 \tau_c$, which is known for stationary, Markovian, Gaussian processes, and also deduced in the Appendix [Eq. (A19)]. We get $T_2 = 1.01$ ms. This value doubles the one previously obtained for the magnetic field orientation ($\theta = 45°, \phi = 49°$).[29] The rise is due to the partial ZEFOZ effect discussed in the previous section. It is worth noting that σ_Δ is a parameter that is dependent on the magnetic field orientation. On the other hand, τ_c is independent, providing us with a more general piece of information about the system.

With the information gathered so far, we know that π pulses that are spectrally wide enough and much shorter than τ_c are feasible in Tm^{3+}:YAG. This enables the design of CPMG sequences aimed at extending T_2. In the next section, we will show initial evidence that this is indeed possible.

B. CPMG experiments with a few π pulses

First we prepare the system by optically pumping the crystal into a single energy sublevel of the nuclear spin over an optical interval that is ∼400 kHz broad. Then, we apply a CPMG sequence, as sketched in Fig. 5(a). It starts by a $\pi/2$ pulse, which transforms the initial population difference into a coherence (i.e., rotation of the Bloch vectors from the vertical axis to the transverse plane of the Bloch sphere). A sequence of n π pulses follows, arriving at instants $t_j = (2j+1)\tau/2$ ($j = 0, \ldots, n-1$) with phases $[1 + (-1)^{j+1}]\pi/2$. They

rephase the spins at instants $j\tau$, with τ being the time interval between two pulses. Just as in the spin-echo experiment, another $\pi/2$ pulse of phase $[1+(-1)^n]\pi/2$ is applied at the end of the sequence to enable the optical detection of the final coherence. Here again, $|\rho_{ab}|$ is recovered from the initial (i.e., right after optical pumping) and final transmitted probe intensity.

We have performed two preliminary experiments to test the action of the CPMG sequence onto ρ_{ab}. In the first one, n was increased while the total free evolution time of the sequence, $n\tau$, was kept fixed at 2 ms. The results are exhibited in Fig. 5(b). We observe that $|\rho_{ab}|$ rises as n is increased (τ is shortened), providing evidence of the preservation of ρ_{ab} by the CPMG sequence. Our theoretical model (hollow squares) matches the experimental data (solid squares) very well for the same τ_c and σ_Δ obtained from the fit of the spin-echo data (Fig. 4). For large n, $|\rho_{ab}|$ seems to tend to a stationary behavior. In fact, the rightmost data point in Fig. 5(b) is close to τ_c. A plateaulike behavior is better defined in Fig. 5(c). Here, n is fixed to 4 and τ is varied through τ_c. We see that as τ is shortened, $|\rho_{ab}|$ increases until it reaches a plateau (the fact that $|\rho_{ab}|$ does not attain unity for $\tau \to 0$ is probably due to the reasons mentioned in the analysis of Fig. 4). This behavior allows us to distinguish between two regimes. In fact, the borderline is in good agreement with the previously obtained value $\tau_c = 172$ μs. For $\tau > \tau_c$, Δ fluctuates significantly during one elementary sequence of the CPMG process [dashed rectangle in Fig. 5(a)]. In such a case, the CPMG strategy fails at keeping ρ_{ab}. For $\tau < \tau_c$, the elementary sequence is short enough to ensure that the decoherence is suppressed or, at least, strongly diminished.

C. Extension of the coherence lifetime

Let us now turn to experiments aimed at keeping the coherence over long time intervals. In Fig. 6, we show $|\rho_{ab}|$ as a function of $n\tau$ (total free evolution time) for CPMG sequences with a large number of pulses and for different values of τ. Each data set labeled $\tau = 150$, 100, 10, and 3 μs has been obtained by increasing n for a fixed value of τ. In the figure, we also include the standard spin-echo measurement (labeled $n = 1$) for comparison. We observe that the data sets display a linear behavior in log scale. This translates the fact that the time scale involved is much longer than τ_c [see the Appendix, especially Eq. (A16)]. The slope, defined as T_2^{-1}, decreases significantly for decreasing τ. The maximum T_2 attained is (230 ± 30) ms, for $\tau = 3$ μs. That is more than 220 times larger than the value obtained through the standard spin echo, and 450 times larger than the one measured for a magnetic field orientation ($\theta = 49°, \phi = 45°$) that does not satisfy any $\partial_\alpha \Delta = 0$ ($\alpha = \theta, \phi$) condition[29] (i.e., absence of partial ZEFOZ effect). These results prove the T_2 extension in Tm^{3+}:YAG provided by the application of a CPMG sequence with $\tau < \tau_c$.

In Fig. 7, we plot the values of T_2 obtained from a least-squares fit to the data of Fig. 6. The figure also displays the theoretical prediction for T_2 according to Eq. (A16). We see that the overall experimental and theoretical behaviors are similar. However, the experimental T_2 is always lower than the predicted one. For $\mu = 150$ μs, experimental and theoretical values are 15.4 and 18.7 ms, respectively. However, for $\mu = 3$ μs, the corresponding values are 0.230 and 43 s. The ratio theory/experiment is not far from unity for large values of τ, but it attains 190 for $\tau = 3$ μs. This is partly due to the cumulated imperfections of the spin rephasing by one single elementary sequence. For $\tau = 150$ μs, only 100 elementary sequences are applied to reach 15 ms of free evolution, but for $\tau = 3$ μs, 5000 sequences are necessary. In addition to this source of discrepancy between experiment and theory, it is worth recalling that we have made use of a very simple model of decoherence in virtue of its straightforward mathematical treatment (see the Appendix). This model assigns decoherence to fluctuations of the spin-transition frequency only. The latter quantity is defined as a stationary, Markovian, Gaussian

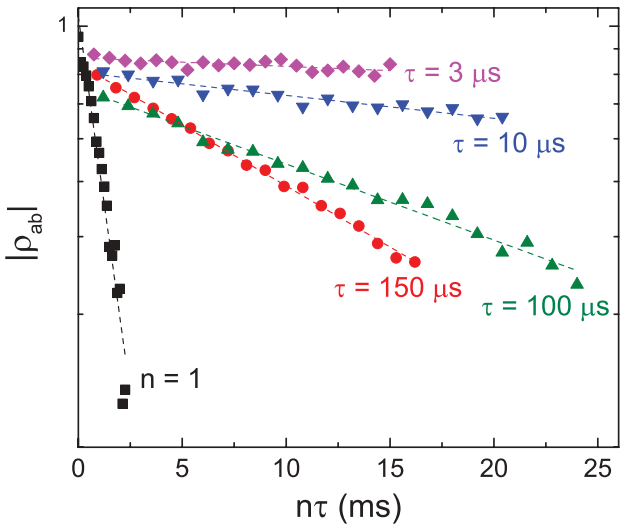

FIG. 6. (Color online) Measurement of T_2 through CPMG sequences with different τ values. For data sets labeled $\tau = 150$, 100, 10, and 3 μs, τ is kept fixed and n is increased. The data set labeled $n = 1$ is a standard spin-echo experiment (n is fixed and τ is increased). The dashed lines result from least-squares fits.

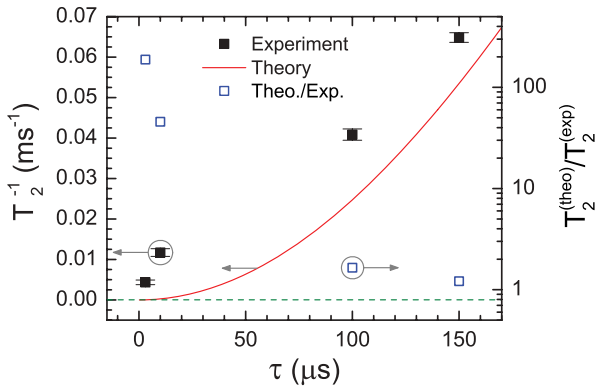

FIG. 7. (Color online) CPMG-extended T_2 as a function of τ. The experimental values (solid black symbols) result from the least-squares fit of the data of Fig. 6. The theoretical prediction (solid red line) represents Eq. (A16). The green dashed line indicates the lower bound $(2T_1)^{-1}$ ($T_1 \sim 1$ min). The ratio between theoretical and experimental T_2 values is also plotted (hollow blue symbols; these data refer to the right vertical axis).

stochastic process, which are three properties that suffice for complete characterization. We estimate that spin-spin interactions between the impurity ion and the spin bath of the crystal (other than those of the *flip-flop* and frozen-core kinds) can be reasonably classed as stationary and Markovian. However, the qualification of Gaussian, taken only because of the analytical resolution it provides, is questionable and would need further consideration. In addition, spin-lattice interactions, for instance, of rarer occurrence and responsible for T_1 (measured to be $\sim$1 min), are not at all taken into account in our model. Flip-flop and frozen-core interactions are discarded as well. When looking at long times, which becomes possible thanks to the DD compensation for spin-spin decoherence, these effects become dominant. This, together with the uncertainty of the Gaussian assumption, might explain the discrepancy with the experimental results. Other relaxation sources not accounted for in our calculations can be invoked, such as crystal heating or instantaneous spectral diffusion by the rf pulses. Further investigation is needed to estimate the potential impact of those effects.

IV. CONCLUSIONS

π-pulse-based DD techniques in Tm^{3+}:YAG posed the problem of high rf power requirements imposed by the large inhomogeneous broadening of the spin transition. We have shown that it is possible to minimize this broadening by carefully choosing an orientation for the static magnetic field such that the sensitivity of the spin-transition frequency to the field orientation is minimal. In this way, a large span in magnetic field orientation seen by spins at different sites in the lattice translate into a small span of transition frequencies. The inhomogeneous broadening has been reduced by a factor $\geqslant$5. At the same time, T_2 has been doubled as a consequence of a partial ZEFOZ effect. π pulses that are effective over the whole inhomogeneous line are now feasible in Tm^{3+}:YAG with reasonable rf powers. This has enabled the application of a CPMG DD sequence. We have observed a clear increase in T_2 as the time length of the elementary sequence in the CPMG protocol was reduced. A maximum value of (227 ± 30) ms was obtained. It represents a 445-fold rise with respect to previous experimental values. A simple theoretical model that we proposed showed excellent agreement with our experimental data for sequences with few pulses ($\sim$10). It allowed the extraction of the parameters that characterize the fluctuation: its standard deviation and its correlation time, estimated to (2.3 ± 0.2) kHz and (172 ± 30) μs (at 1.7 K), respectively. The comparison between experiment and model declines as the number of pulses is increased. We assume that this is due to the accumulation of pulse imperfections and to decoherence mechanisms that are disregarded in the model.

ACKNOWLEDGMENTS

This research has been supported by the European Commission through Projects No. FP7-QuReP(STREP-247743) and No. FP7-CIPRIS(MC ITN-287252), by the Agence Nationale de la Recherche through Project No. ANR-09-BLAN-0333-03 and by the Direction Générale de l'Armement.

APPENDIX

Here we aim at calculating the evolution of the coherence during a CPMG sequence. We will consider an inhomogeneously broadened atomic transition centered at Δ_0. Each ion in the inhomogeneous line suffers from crystal-field fluctuations that induce fluctuations in its spin-transition frequency. Its detuning from the line center varies as

$$\delta(t) = \bar{\delta} + \zeta(t), \tag{A1}$$

where $\bar{\delta}$ is the time-averaged detuning. We assume the initial situation $(t = 0)$ in which the coherence $\rho_{ab}(t = 0) = \rho_{ab}^{(0)}$ is the same for all of the ions, and there is no population difference (i.e., all Bloch vectors aligned along an axis contained in the transverse plane of the Bloch sphere). This scenario can be reached, for example, by emptying one of the levels of the spin transition (optical pumping) and applying a rf $\pi/2$ pulse, as done in the experiments described above.

The CPMG sequence consists of a succession of n π pulses. The π pulses are applied at instants $t = (2j + 1)\tau/2$, $j = 0, \ldots, n - 1$. We are interested in the echo intensity at $t = n\tau$. This is proportional to the coherence averaged over the inhomogeneous distribution, $\tilde{\rho}_{ab}$. As each π pulse of the sequence conjugates the coherences, in the reference frame rotating at angular frequency Δ_0, $\tilde{\rho}_{ab}$ is given by

$$\tilde{\rho}_{ab}(n,\tau) = \rho_{ab}^{(0)} \int d\bar{\delta} g(\bar{\delta}) \Big\langle \exp\left\{ i \int_{(2n-1)\frac{\tau}{2}}^{n\tau} dt\delta(t) - \left[i \int_{(2n-3)\frac{\tau}{2}}^{(2n-1)\frac{\tau}{2}} dt\delta(t) - \left(\cdots - \left\{ i \int_{3\frac{\tau}{2}}^{5\frac{\tau}{2}} dt\delta(t) - \left[i \int_{\frac{\tau}{2}}^{3\frac{\tau}{2}} dt\delta(t) - i \int_{0}^{\frac{\tau}{2}} dt\delta(t) \right] \right\} \right) \right] \right\} \Big\rangle, \tag{A2}$$

$$\tilde{\rho}_{ab}(n,\tau) = \rho_{ab}^{(0)} \Big\langle \exp\left\{ i \left[\int_{(2n-1)\frac{\tau}{2}}^{n\tau} dt\zeta(t) + (-1) \int_{(2n-3)\frac{\tau}{2}}^{(2n-1)\frac{\tau}{2}} dt\zeta(t) + \cdots + (-1)^{n-2} \int_{3\frac{\tau}{2}}^{5\frac{\tau}{2}} dt\zeta(t) + (-1)^{n-1} \times \int_{\frac{\tau}{2}}^{3\frac{\tau}{2}} dt\zeta(t) + (-1)^{n} \int_{0}^{\frac{\tau}{2}} dt\zeta(t) \right] \right\} \Big\rangle, \tag{A3}$$

where $g(\bar{\delta})$ stands for the inhomogeneous distribution and $\langle \cdot \rangle$ represents the statistical average. For going from Eq. (A2) to Eq. (A3), we have taken into account that the contribution from $\bar{\delta}$ cancels out. Equation (A3) can be written as

$$\tilde{\rho}_{ab}(n,\tau) = \rho_{ab}^{(0)} \left\langle e^{i \int_0^{n\tau} dt\, s_\tau(t)\zeta(t)} \right\rangle, \tag{A4}$$

with

$$s_\tau(t) = \begin{cases} (-1)^n & 0 < t < \frac{\tau}{2} \\ (-1)^{n-j} & (2j-1)\frac{\tau}{2} < t < (2j+1)\frac{\tau}{2} \\ 1 & (2n-1)\frac{\tau}{2} < t < n\tau, \end{cases} \tag{A5}$$

where $j = 1, \ldots, n-1$.

Let $\zeta(t)$ be a stationary, Gaussian, Markovian process. According to Doob's theorem,[37] only the Ornstein-Uhlenbeck[38] process simultaneously satisfies those three assumptions. The corresponding autocorrelation function reads

$$\langle \zeta(t)\zeta(t') \rangle = \sigma_\Delta^2 e^{-|t-t'|/\tau_c}, \tag{A6}$$

where σ_Δ and τ_c represent the standard deviation of the fluctuation and the correlation time, respectively. Since $\zeta(t)$ is a Gaussian process, it can be shown that

$$\left\langle e^{i\int_{t_0}^{t} dt' f(t')\zeta(t')} \right\rangle = e^{-\frac{1}{2}\langle [\int_{t_0}^{t} dt' f(t')\zeta(t')]^2 \rangle}. \tag{A7}$$

With this in mind, the expression for the coherence reduces to

$$\tilde{\rho}_{\mathrm{ab}}(n,\tau) = \rho_{\mathrm{ab}}^{(0)} e^{-\gamma(n,\tau)}, \tag{A8}$$

with

$$\gamma(n,\tau) = \frac{1}{2}\left\langle \left[\int_0^{n\tau} dt' s_\tau(t)\zeta(t) \right]^2 \right\rangle. \tag{A9}$$

Let us perform the calculation for $\gamma(n,\tau)$:

$$\gamma(n,\tau) = \frac{1}{2}\int_0^{n\tau} dt \int_0^{n\tau} dt' s_\tau(t) s_\tau(t') \langle \zeta(t)\zeta(t') \rangle, \tag{A10}$$

$$= \frac{\sigma_\Delta^2}{2}\int_0^{n\tau} dt \int_0^{n\tau} dt' s_\tau(t) s_\tau(t') e^{-|t-t'|/\tau_c}. \tag{A11}$$

The above double integral simplifies if we consider the relation $\int_{t_0}^{t} dt' \int_{t_0}^{t} dt'' f(t',t'') = 2\int_{t_0}^{t} dt' \int_{t_0}^{t'} dt'' f(t',t'')$, which is valid for any $f(t',t'')$ symmetric after permutation of t' and t''. We therefore get

$$\gamma(n,\tau) = \sigma_\Delta^2 \int_0^{n\tau} dt \int_0^{t} dt' s_\tau(t) s_\tau(t') e^{-(t-t')/\tau_c}, \tag{A12}$$

$$= \sigma_\Delta^2 \int_0^{n\tau} dt\, s_\tau(t) h_\tau(t), \tag{A13}$$

with

$$h_\tau(t) = (-1)^n (\sigma_\Delta \tau_c)^2 e^{-\frac{t}{\tau_c}} \begin{cases} (e^{\frac{t}{\tau_c}} - 1) & 0 < t < \frac{\tau}{2} \\ \left\{ e^{\frac{\tau}{2\tau_c}} - 1 - \frac{e^{\frac{\tau}{\tau_c}}-1}{e^{\frac{\tau}{\tau_c}}+1} e^{\frac{\tau}{2\tau_c}} [1 + (-1)^j e^{(j-1)\frac{\tau}{\tau_c}}] \right. & \\ \quad \left. + (-1)^j (e^{\frac{t}{\tau_c}} - e^{(2j-1)\frac{\tau}{2\tau_c}}) \right\} & (2j-1)\frac{\tau}{2} < t < (2j+1)\frac{\tau}{2} \\ \left\{ e^{\frac{\tau}{2\tau_c}} - 1 - \frac{e^{\frac{\tau}{\tau_c}}-1}{e^{\frac{\tau}{\tau_c}}+1} e^{\frac{\tau}{2\tau_c}} [1 + (-1)^n e^{(n-1)\frac{\tau}{\tau_c}}] \right. & \\ \quad \left. + (-1)^n (e^{\frac{t}{\tau_c}} - e^{(2j-1)\frac{\tau}{2\tau_c}}) \right\} & (2n-1)\frac{\tau}{2} < t < n\tau, \end{cases} \tag{A14}$$

where j runs from 1 through $n-1$. By computing the integral in Eq. (A13), we obtain the final expression for $\gamma(n,\tau)$:

$$\gamma(n,\tau) = (\sigma_\Delta \tau_c)^2 \left\{ \left[\frac{1}{\tau_c} - \frac{2}{\tau} \tanh\left(\frac{\tau}{2\tau_c} \right) \right] t - [1 + (-1)^{n+1} e^{-t/\tau_c}] \left[1 - \operatorname{sech}\left(\frac{\tau}{2\tau_c} \right) \right]^2 \right\}. \tag{A15}$$

It is understood in Eq. (A15) that $t = n\tau$.

We see from Eq. (A15) that the coherence does not decay in an exponential manner. However, the exponential behavior is recovered in the $t \gg \tau_c$ limit, with a characteristic time given by

$$T_2^{-1}(\tau) = \sigma_\Delta^2 \tau_c \left[1 - \frac{2\tau_c}{\tau} \tanh\left(\frac{\tau}{2\tau_c} \right) \right], \quad t \gg \tau_c. \tag{A16}$$

Moreover, if $\tau \ll \tau_c$, then T_2 reduces to

$$T_2^{-1}(\tau) = \frac{1}{12} \frac{\sigma_\Delta^2 \tau^2}{\tau_c}, \quad t \gg \tau_c \gg \tau. \tag{A17}$$

From Eq. (A15), we can easily calculate the coherence lifetime obtained by a single spin echo by assigning $n = 1$ and $\tau = t$. This yields

$$\gamma_{\mathrm{se}}(t) = (\sigma_\Delta \tau_c)^2 \left(\frac{t}{\tau_c} + 4e^{-\frac{t}{2\tau_c}} - e^{-\frac{t}{\tau_c}} - 3 \right). \tag{A18}$$

In the limit $t \gg \tau_c$, we get the standard result

$$\gamma_{\mathrm{se}}(t) = \sigma_\Delta^2 \tau_c t, \quad t \gg \tau_c. \tag{A19}$$

It is worth mentioning that the development described here to obtain $\gamma(n,\tau)$ is analogous to the extension to n π pulses of the calculation performed by Herzog and Hahn in Ref. 39 for one π pulse. The same result is found.

[1] W. Tittel, M. Afzelius, T. Chanelière, R. Cone, S. Kröll, S. Moiseev, and M. Sellars, Laser Photon. Rev. **4**, 244 (2010).

[2] A. I. Lvovsky, B. C. Sanders, and W. Tittel, Nature (London) **3**, 706 (2009).

[3] G. Liu and B. Jacquier, in *Spectroscopic Properties of Rare Earths in Optical Materials*, edited by G. Liu and B. Jacquier, Vol. 83 (Springer, Berlin, 2005).

[4] I. Solomon, C. R. Acad. Sci. Paris **248**, 92 (1959).

[5] S. R. Hartmann and E. L. Hahn, Phys. Rev. **128**, 2042 (1962).

[6] E. Fraval, M. J. Sellars, and J. J. Longdell, Phys. Rev. Lett. **92**, 077601 (2004).

[7] M. Lovrić, P. Glasenapp, D. Suter, B. Tumino, A. Ferrier, P. Goldner, M. Sabooni, L. Rippe, and S. Kröll, Phys. Rev. B **84**, 104417 (2011).

[8] W. Yang, Z.-Y. Wang, and R.-B. Liu, Frontiers Phys. **6**, 2 (2011).

[9] E. L. Hahn, Phys. Rev. **80**, 580 (1950).

[10] M. Mehring, *Principles of High Resolution NMR in Solids*, 2nd ed. (Springer-Verlag, Berlin, 1983).

[11] L. Viola and S. Lloyd, Phys. Rev. A **58**, 2733 (1998).

[12] M. Ban, J. Mod. Opt. **45**, 2315 (1998).

[13] P. Zanardi, Phys. Lett. A **258**, 77 (1999).

[14] L. Viola, E. Knill, and S. Lloyd, Phys. Rev. Lett. **82**, 2417 (1999).

[15] H. Y. Carr and E. M. Purcell, Phys. Rev. **94**, 630 (1954).

[16] S. Meiboom and D. Gill, Rev. Sci. Instrum. **29**, 688 (1958).

[17] J. J. L. Morton, A. M. Tyryshkin, A. Ardavan, S. C. Benjamin, K. Porfyrakis, S. A. Lyon, and G. A. D. Briggs, Nature Phys. **2**, 40 (2006).

[18] M. J. Biercuk, H. Uys, A. P. VanDevender, N. Shiga, W. M. Itano, and J. J. Bollinger, Nature (London) **458**, 996 (2009).

[19] J. Du, X. Rong, N. Au Zhao, Y. Wang, J. Yang, and R. B. Liu, Nature (London) **461**, 1265 (2009).

[20] R. M. Macfarlane, Opt. Lett. **18**, 1958 (1993).

[21] M. Bonarota, J.-L. Le Gouët, and T. Chanelière, New J. Phys. **13**, 013013 (2011).

[22] F. de Seze, A. Louchet, V. Crozatier, I. Lorgeré, F. Bretenaker, J.-L. Le Gouët, O. Guillot-Noël, and P. Goldner, Phys. Rev. B **73**, 085112 (2006).

[23] A. Louchet, J. S. Habib, V. Crozatier, I. Lorgeré, F. Goldfarb, F. Bretenaker, J.-L. Le Gouët, O. Guillot-Noël, and Ph. Goldner, Phys. Rev. B **75**, 035131 (2007).

[24] A. Louchet, Y. Le Du, F. Bretenaker, T. Chanelière, F. Goldfarb, I. Lorgeré, J.-L. Le Gouët, O. Guillot-Noël, and P. Goldner, Phys. Rev. B **77**, 195110 (2008).

[25] R. Lauro, T. Chanelière, and J.-L. Le Gouët, Phys. Rev. A **79**, 053801 (2009).

[26] R. Lauro, T. Chanelière, and J. L. Le Gouët, Phys. Rev. A **79**, 063844 (2009).

[27] T. Chanelière, J. Ruggiero, M. Bonarota, M. Afzelius, and J.-L. Le Gouët, New J. Phys. **12**, 023025 (2010).

[28] M. Bonarota, J. Ruggiero, J.-L. Le Gouët, and T. Chanelière, Phys. Rev. A **81**, 033803 (2010).

[29] R. Lauro, T. Chanelière, and J.-L. Le Gouët, Phys. Rev. B **83**, 035124 (2011).

[30] A. Abragam and B. Bleaney, *Electronic Paramagnetic Resonance of Transition Ions*, Chap. 15 (Clarendon, Oxford, 1970).

[31] K. Holliday, M. Croci, E. Vauthey, and U. P. Wild, Phys. Rev. B **47**, 14741 (1993).

[32] B. S. Ham, M. S. Shahriar, M. K. Kim, and P. R. Hemmer, Phys. Rev. B **58**, R11825 (1998).

[33] J. J. Longdell, A. L. Alexander, and M. J. Sellars, Phys. Rev. B **74**, 195101 (2006).

[34] R. M. Macfarlane and R. M. Shelby, in *Spectroscopy of Solids Containing Rare Earth Ions*, edited by A. Kaplyanskii and R. M. Macfarlane Vol. 21 (North-Holland, Amsterdam, 1987).

[35] M. A. Teplov, Zh. Eksp. Teor. Fiz. **53**, 1510 (1967) [Sov. Phys. JETP **26**, 872 (1968)] .

[36] Y. Sun, G. M. Wang, R. L. Cone, R. W. Equall, and M. J. M. Leask, Phys. Rev. B **62**, 15443 (2000).

[37] J. L. Doob, Ann. Math. Sec. Ser. **43**, 351 (1942).

[38] G. E. Uhlenbeck and L. S. Ornstein, Phys. Rev. **36**, 823 (1930).

[39] B. Herzog and E. L. Hahn, Phys. Rev. **103**, 148 (1956).